Available online at www.sciencedirect.com
SCIENCE DIRECT®
Journal of Theoretical Biology 231 (2004) 443–458
Journal of Theoretical Biology
www.elsevier.com/locate/yjtbi

Modeling the synchronization of yeast respiratory oscillations

Michael A. Henson*

Department of Chemical Engineering, University of Massachusetts, Amherst, MA 01003-9303, USA

Received 13 April 2004; received in revised form 30 June 2004; accepted 12 July 2004
Available online 11 September 2004

Abstract

The budding yeast *Saccharomyces cerevisiae* exhibits autonomous oscillations when grown aerobically in continuous culture with ethanol as the primary carbon source. A single cell model that includes the sulfate assimilation and ethanol degradation pathways recently has been developed to study these respiratory oscillations. We utilize an extended version of this single cell model to construct large cell ensembles for investigation of a proposed synchronization mechanism involving hydrogen sulfide. Ensembles with as many as 10,000 cells are used to simulate population synchronization and to compute transient number distributions from asynchronous initial cell states. Random perturbations in intracellular kinetic parameters are introduced to study the synchronization of single cells with small variations in their unsynchronized oscillation periods. The cell population model is shown to be consistent with available experimental data and to provide insights into the regulatory mechanisms responsible for the synchronization of yeast metabolic oscillations.

Keywords: Yeast cell population; Oscillatory dynamics; Cellular synchronization; Metabolic regulation; Cell population model

1. Introduction

The budding yeast *Saccharomyces cerevisiae* exhibits sustained oscillations when grown in continuous culture under certain environmental conditions. The oscillations are autonomous in the sense that external forcing is not required to establish or maintain the limit cycle dynamics. Three distinct types of autonomous yeast oscillations have been reported: glycolytic oscillations (Aon et al., 1992; Ghosh et al., 1971), respiratory oscillations (Keulers et al., 1996a, b), and cell cycle related oscillations (von Meyenburg, 1973; Parulekar et al., 1986). Improved understanding of the cellular mechanisms involved could yield important insights into dynamic regulation of metabolism in yeast cells and in eukaryotic cells present in higher organisms. Glycolytic and respiratory oscillations are more amenable to theoretical analysis because the limit cycle dynamics are attributable to cellular metabolism and independent of cell cycle progression. A number of experimental (Das and Busse, 1991; Ghosh and Chance, 1964) and modeling (Bier et al., 2000; Wolf and Heinrich, 2000) studies have attempted to decipher the metabolic determinants of glycolytic oscillations. These studies support the hypothesis that an autocatalytic reaction involving the glycolytic enzyme phosphofructokinase causes single cells oscillations. A negative feedback mechanism in the sulfate assimilation pathway is thought to be responsible for respiratory oscillations at the individual cell level (Sohn and Kuriyama, 2001).

Single cell oscillations must be synchronized to be observable at the population level. A perfectly synchronized population is an idealized concept in which every cell oscillates with exactly the same phase and amplitude. Actual experiments yield partially synchronized populations comprised of oscillating cells with narrowly distributed phases and amplitudes. In addition to studying the emergent dynamics of coupled cellular oscillators, synchronized cultures are commonly used to

*Tel.: 1-413-545-3481, fax: +1-413-545-1647.
E-mail address: henson@ecs.umass.edu (M.A. Henson).

0022-5193/$ - see front matter © 2004 Elsevier Ltd. All rights reserved.
doi:10.1016/j.jtbi.2004.07.009

investigate cellular metabolism because population averaged measurements are representative of single cell behavior (Muller et al., 2003). Population synchronization requires some form of communication between individual cells. The synchronization mechanisms proposed for glycolytic and respiratory oscillations both involve an intracellular species produced by single cells and excreted into the extracellular environment. Acetaldehyde is believed to be the synchronizing agent for glycolytic oscillations (Richard et al., 1996, 1994), while recent experiments implicate hydrogen sulfide in the synchronization of respiratory oscillations (Sohn and Kuriyama, 2001; Sohn et al., 2000).

Theoretical analysis of cellular synchronization motivates the development of dynamic population models which capture single cell metabolism. Population balance equation (PBE) models (Fredrickson et al., 1967; Henson, 2003b; Hjortso and Nielsen, 1995) commonly used to describe microbial cell population dynamics are not well suited for the incorporation of metabolic reaction pathways. While metabolically structured PBE models can be formulated if the intracellular reaction stoichiometry and kinetics are known (Nielsen and Villadsen, 1994), we have shown that the high dimension of the intracellular state space renders such PBE models computationally intractable (Henson et al., 2002). Several investigators have used small ensembles of single cell models to study the synchronization of glycolytic oscillations (Bier et al., 2000; Wolf and Heinrich, 2000; Wolf et al., 2000). Each of these studies is severely limited by the very small number of cells included in the ensemble. In particular, cellular distributions which are readily obtained from PBE models cannot be reliably computed with ensembles consisting of a few individual cells (Henson et al., 2002).

Based on previous work for *E. coli* cultures (Domach and Shuler, 1984; Kim and Shuler, 1990), we recently developed a cell population model comprised of 1000 metabolically structured cells to study the synchronization of yeast glycolytic oscillations (Henson et al., 2002). A single cell model and synchronization mechanism previously developed (Wolf and Heinrich, 2000) were used in our investigations. Although the cell population model was comprised of 6000 nonlinear ordinary differential equations, an efficient numerical solution strategy was developed by exploiting the approximately banded structure of the model equations. Random variations in the initial state and/or intracellular kinetic parameters of individual cells produced complex synchronization dynamics not adequately captured by small ensembles. Transient cell number distributions were computed from ensemble simulation data by discretization of the intracellular state. An inherent limitation of this modeling approach is that achievable resolution of the population dynamics is limited by the number of cells included in the ensemble.

The primary goal of this paper is to utilize the cell ensemble modeling framework to study the synchronization of yeast respiratory oscillations. A synchronization mechanism proposed by experimentalists (Sohn and Kuriyama, 2001; Sohn et al., 2000) involving hydrogen sulfide mediated inhibition of the respiratory chain is evaluated. Theoretical analysis is based on an extended version of a previously developed single cell model (Wolf et al., 2001) which is derived by adding hydrogen sulfide membrane transport and accumulation in the extracellular environment. A secondary objective is to demonstrate that the proposed modeling framework is applicable to more complex cell models and larger ensembles than those used in our previous study of glycolytic oscillations (Henson et al., 2002). Ensembles with as many as 10,000 individual cells are used to simulate population synchronization and to compute transient number distributions. Two general scenarios are considered: (1) synchronization of structurally identical cells that are initialized to represent varying degrees of population asynchrony; and (2) synchronization of non-identical cells with small random variations in their intracellular kinetic parameters. Model predictions are qualitatively compared to available experimental data to assess the validity of the hypothesized synchronization mechanism. A few preliminary simulation results were included in a recent review paper by the author (Henson, 2004).

2. Previous work on yeast respiratory oscillations

2.1. Experimental studies

Respiratory oscillations are observed when the yeast *S. cerevisiae* is grown aerobically in continuous culture with glucose (Satroutdinov et al., 1992), ethanol (Keulers et al., 1996b) or acetaldehyde (Keulers and Kuriyama, 1998) as the primary carbon source. Sustained oscillations have been reported in many extracellular variables including the rates of oxygen uptake, sulfate uptake and carbon dioxide production and the concentrations of ethanol, acetate, acetaldehyde and hydrogen sulfide (Sohn and Kuriyama, 2001; Satroutdinov et al., 1992). Intracellular variables such as pH and the concentrations of acetate, glutathione, ATP and NADH also have been shown to exhibit oscillatory dynamics (Sohn and Kuriyama, 2001; Satroutdinov et al., 1992). The oscillation period is approximately 40–60 min in glucose and ethanol media (Satroutdinov et al., 1992; Murray et al., 2001).

Sulfate assimilation and ethanol degradation are essential components of the synchronization mechanism in ethanol media. The sulfate assimilation pathway

produces the amino acid cysteine, which inhibits sulfate assimilation at high concentrations (Sohn and Kuriyama, 2001), and hydrogen sulfide, which inhibits the respiratory chain (Sohn et al., 2000). Inhibition of sulfate assimilation metabolism by cysteine has been proposed to be the primary cause of single cell oscillations (Sohn and Kuriyama, 2001). This hypothesis is supported by experiments that showed the oscillation period was inversely proportional to the extracellular sulfate concentration and the oscillatory dynamics were completely eliminated when the original media was replaced with sulfate-free media (Sohn and Kuriyama, 2001). The ethanol degradation pathway also plays a critical role as its intermediate O-acetylhomoserine is a precursor for cysteine synthesis. Oscillations in the sulfate assimilation pathway are believed to be propagated to the respiratory chain by inhibition of oxidative phosphorylation by hydrogen sulfide (Sohn et al., 2000).

Experiments in which autonomous oscillations were eliminated at high gas flow rates suggest that the synchronizing agent is a volatile species excreted by individual cells and removed from the gas phase via the purge stream (Keulers et al., 1996a). Due to its strong influence on intracellular pH, carbon dioxide was originally hypothesized to be the synchronizing species (Keulers et al., 1996a). More recent experiments suggest that hydrogen sulfide mediates population synchrony through inhibition of the respiratory chain (Sohn and Kuriyama, 2001; Sohn et al., 2000). Pulse injections of crystalline sodium sulfide (which was converted to hydrogen sulfide in solution) strongly affected the period of hydrogen sulfide oscillations and their phase relationship with oxygen oscillations (Sohn et al., 2000). A dual synchronization mechanism involving both hydrogen sulfide and acetaldehyde also has been proposed (Murray et al., 2001). The cessation of sustained oscillations in these experiments has been attributed to lack of population synchronization rather than elimination of single cell oscillations.

2.2. Single cell modeling

The cell population model used in this paper to investigate the synchronization of yeast respiratory oscillations is based a previously developed single cell model (Wolf et al., 2001). Fig. 1 shows the metabolic network used for derivation of the single cell model. The following cellular processes considered to be essential for oscillations in ethanol media were considered: (1) sulfate update and degradation in the cytosol resulting in the production of hydrogen sulfide (H_2S) and cysteine; (2) ethanol uptake and degradation in the cytosol resulting in precursors for cysteine production and the citrate acid cycle; (3) oxidative phosphorylation in the mitochondria including the influx/outflux of oxygen and lumped processes of respiration; (4) the citrate acid cycle in the mitochondria; and (5) ATP transport and consuming processes in the cytosol and

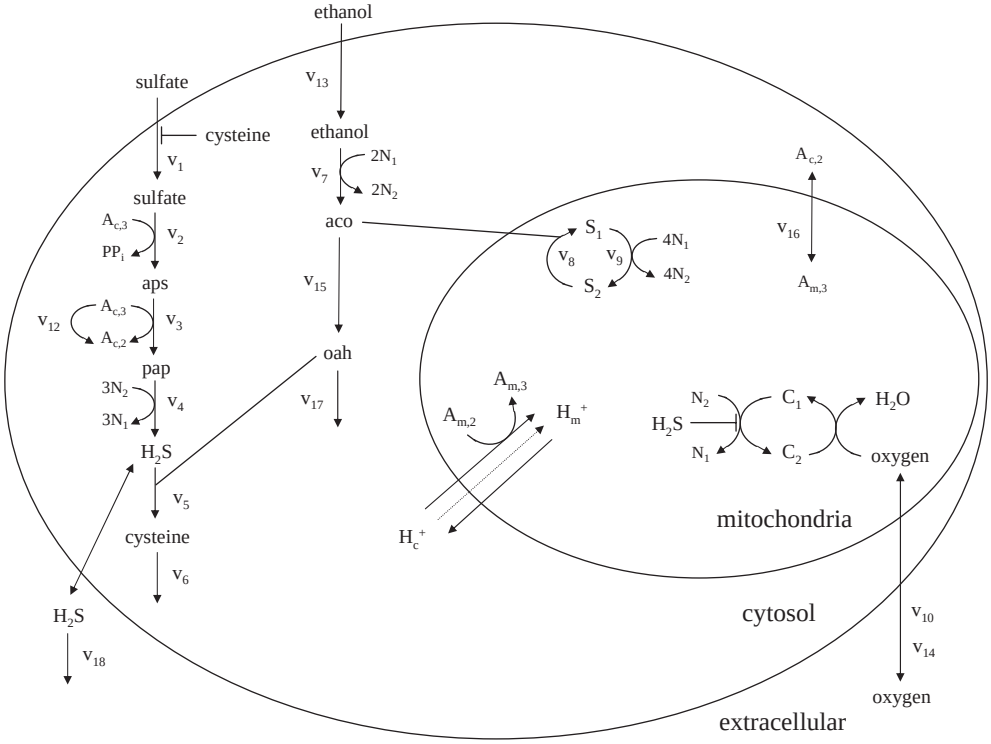

Fig. 1. Metabolic network for modeling synchronization of yeast respiratory oscillations.

mitochondria. Key regulatory effects included in the cell model were the inhibition of sulfate uptake by cysteine and the inhibition of respiration by hydrogen sulfide. The citrate acid cycle intermediates (S_1, S_2) as well as the co-enzymes NAD^+/NADH (N_1/N_2), cytosolic ADP/ATP ($A_{c,2}/A_{c,3}$) and mitochondrial ADP/ATP ($A_{m,2}/A_{m,3}$) were assumed to be conserved moieties.

A dynamic cell model consisting of 13 nonlinear ordinary differential equations was derived by formulating mass balances for the independent chemical species in the metabolic network (Wolf et al., 2001). Due to a lack of experimental data, the kinetic parameters were chosen heuristically to yield sustained oscillations with a period of approximately 40 dimensionless time units. The single cell model was numerically integrated to investigate the ability of the proposed regulatory mechanisms to generate autonomous oscillations consistent with experimental observations. The major conclusions of this theoretical study were: (1) inhibition of sulfate uptake by cysteine produced strong oscillations in the intermediates of sulfur metabolism even in the absence of respiratory inhibition; (2) inhibition of oxidative phosphorylation by hydrogen sulfide caused the oscillations to spread throughout the entire metabolic network; (3) the oscillation period decreased with increasing sulfate uptake and stationary solutions were obtained when the uptake was sufficiently low; and (4) while the phase relationships between most variables were captured, the model incorrectly predicted that the adenine nucleotides ($A_{c,3}, A_{m,3}$) oscillated 180° out of phase with oxygen.

3. Cell population model

3.1. Synchronization mechanism

In this paper a cell population model based on a modified version of the single cell model described above is developed to investigate the synchronization of yeast respiratory oscillations. Available experimental data suggests that hydrogen sulfide mediates population synchrony by inhibition of the respiratory chain (Sohn and Kuriyama, 2001; Sohn et al., 2000). This hypothesized mechanism is modeled by including a flux term in the single cell model that accounts for transport of hydrogen sulfide across the cell membrane. Unlike the original model in which hydrogen sulfide was assumed to be degraded within the cell (Wolf et al., 2001), the proposed model includes an extracellular hydrogen sulfide balance with a degradation term. Additional extracellular balances on sulfate, ethanol and oxygen are omitted since these species are not directly involved in the synchronization mechanism. The population model is comprised of an ensemble of modified single cell models and the extracellular hydrogen sulfide balance.

The differential equations describing the ith cell in the population are:

$$\frac{dC_{sul,i}}{dt} = v_{1,i} - v_{2,i}, \tag{1}$$

$$\frac{dC_{aps,i}}{dt} = v_{2,i} - v_{3,i}, \tag{2}$$

$$\frac{dC_{pap,i}}{dt} = v_{3,i} - v_{4,i}, \tag{3}$$

$$\frac{dC_{h2s,i}}{dt} = v_{4,i} - v_{5,i} - J_i, \tag{4}$$

$$\frac{dC_{cys,i}}{dt} = v_{5,i} - v_{6,i}, \tag{5}$$

$$\frac{dC_{eth,i}}{dt} = v_{13,i} - v_{7,i}, \tag{6}$$

$$\frac{dC_{aco,i}}{dt} = v_{7,i} - v_{8,i} - v_{15,i}, \tag{7}$$

$$\frac{dC_{S1,i}}{dt} = v_{8,i} - v_{9,i}, \tag{8}$$

$$\frac{dC_{oxy,i}}{dt} = v_{10,i} - v_{11A,i} - v_{14,i}, \tag{9}$$

$$\frac{dC_{A3m,i}}{dt} = v_{11B,i} - v_{16,i}, \tag{10}$$

$$\frac{dC_{N2,i}}{dt} = -3v_{4,i} + 2v_{7,i} + 4v_{9,i} - v_{11A,i}, \tag{11}$$

$$\frac{dC_{A3c,i}}{dt} = -v_{2,i} - v_{3,i} - v_{12,i} + v_{16,i}, \tag{12}$$

$$\frac{dC_{oah,i}}{dt} = -v_{5,i} + v_{15,i} - v_{17,i}, \tag{13}$$

where C denotes molar concentration and the following abbreviations are used: intracellular sulfate (sul), adenylyl sulfate (aps), 3-phosphoadenylyl sulfate (pap), hydrogen sulfide (h2s), cysteine (cys), intracellular ethanol (eth), acetyl-CoA (aco), citrate acid cycle intermediate (S1), intracellular oxygen (oxy), mitochondrial ATP (A3m), NADH (N2), cytosolic ATP (A3c) and O-acetylhomoserine (oah). The uptake rates of oxygen (v_{10}) and ethanol (v_{13}) are assumed to be constant. Excess oxygen is returned to the extracellular environment at a rate v_{14} that depends linearly on the

intracellular oxygen concentration. The reaction rates v_2–v_9 and v_{15}–v_{17} depend linearly on the metabolite(s) and co-enzyme involved in the corresponding intracellular reactions (Wolf et al., 2001). Individual cell oscillations are attributable to inhibition of sulfate uptake by cysteine:

$$v_{1,i} = v_{0,i}\left[1 + \left(1 + \frac{C_{cys,i}}{K_{C,i}}\right)^{n_i}\right]^{-1}, \tag{14}$$

where v_0 is the uptake rate in the absence of inhibition. The reaction rates v_{11A} and v_{11B} for lumped processes of respiration are derived from a minimal model of oxidative phosphorylation (Wolf et al., 2001):

$$v_{11A,i} = \frac{k_{11,i} C_{N2,i} C_{oxy,i} f_{1,i}(C_{h2s,i})}{\alpha_i C_{N2,i} + C_{oxy,i}}, \tag{15}$$

$$v_{11B,i} = 3v_{11A,i}\frac{C_{A2m,i}}{K_{A,i} + C_{A2m,i}}, \tag{16}$$

where inhibition of the respiratory chain by hydrogen sulfide is modeled as

$$f_{1,i}(C_{h2s,i}) = \left[1 + \left(1 + \frac{C_{h2s,i}}{K_{H,i}}\right)^{m_i}\right]^{-1}. \tag{17}$$

The transport rate v_{12} of ATP from the cytosol to the mitochondria is assumed to depend linearly on the cytosolic ATP concentration.

The hydrogen sulfide flux J across the cell membrane is modeled as

$$J_i = \kappa_i(C_{h2s,i} - C_{h2s,ex}), \tag{18}$$

where $C_{h2s,ex}$ is the extracellular hydrogen sulfide concentration and the parameter κ is related to the membrane permeability. A mass balance on extracellular hydrogen sulfide yields

$$\frac{dC_{h2s,ex}}{dt} = \frac{\varphi}{M}\sum_{i=1}^{M} J_i - v_{18}, \tag{19}$$

where M is the total number of cells and φ is the volume fraction of cells. Rather than model the transport of hydrogen sulfide from the liquid phase to the gas phase and its subsequent removal in the purge gas stream, a simplified description where extracellular hydrogen sulfide is degraded at a rate v_{18} is employed. The degradation rate is assumed to depend linearly on $C_{h2s,ex}$. A similar model for extracellular acetaldehyde has been utilized in cell population models for yeast glycolytic oscillations (Wolf and Heinrich, 2000; Henson et al., 2002).

3.2. Model formulation and numerical solution

Nominal values of the model parameters are shown in Table 1 where k_j denotes the kinetic constant for reaction rate v_j and the total concentrations of the citrate acid cycle intermediates (S_1, S_2), redox equivalents (N_1, N_2), cytosolic adenine nucleotides ($A_{c,2}, A_{c,3}$) and mitochondrial adenine nucleotides ($A_{m,2}, A_{cm,3}$) are denoted S, N, A_c and A_m, respectively. Single cell model parameters are identical to those listed in (Wolf et al., 2001) with the exception of the inhibition constant for oxidative phosphorylation which was decreased ($K_H : 0.5 \to 0.15$) to yield experimentally observed synchronization behavior. The cell density (φ) was chosen as in previous modeling studies on yeast glycolytic oscillations (Wolf and Heinrich, 2000; Henson et al., 2002). The remaining extracellular model parameters (κ, k_{18}) were used to tune the rate of synchronization. Due to the lack of experimental data on which to base the kinetic parameter values (Wolf et al., 2001), the dependent variables plotted below have not been ascribed physical units. Consequently, the cell population model is only suitable for generating qualitative predictions for comparison to experimental data. The nominal parameter values in Table 1 produced a synchronized oscillation period of 45 dimensionless units.

Table 1
Nominal parameter values for the yeast cell population model

Parameter	Value	Parameter	Value
v_0	1.6	k_2	0.2
k_3	0.2	k_4	0.2
k_5	0.1	k_6	0.12
k_7	10	k_8	10
k_9	10	v_{10}	80
k_{11}	10	k_{12}	5
v_{13}	4	k_{14}	10
k_{15}	5	k_{16}	10
k_{17}	1	k_{18}	0.25
n	4	m	4
K_A	1	K_C	0.1
K_H	0.15	α	0.1
A_c	2	A_m	2
S	2	N	2
ϕ	0.1	κ	2.0

A dynamic simulation code was developed in FORTRAN using the stiff ordinary differential equation solver DVODE (Brown et al., 1989). The Jacobian matrix was computed numerically by finite difference approximation for simplicity. Simulation output was sampled every minute to obtain adequate resolution of the oscillatory dynamics. As shown below, ensemble averaged variables were not strongly affected by the number of cells included in the ensemble. The motivation for utilizing large cell ensembles was to obtain accurate resolution of transient cell distributions computed from ensemble simulation data. Our previous work on yeast glycolytic oscillations demonstrated that even 1000 cells

may not be sufficient to produce smooth distributions (Henson et al., 2002).

Most of the dynamic simulation results presented below were generated with 10,000 cells or $n = 13M + 1 = 130,001$ nonlinear ordinary differential equations. The full Jacobian matrix contained 1.69×10^{10} elements that required finite difference approximation each time the model evaluation subroutine was called by the differential equation solver. Brute force integration of this very large differential equation system proved to be computationally infeasible. Efficient model solution was achieved by replacing the full Jacobian matrix with a highly banded approximation (Henson et al., 2002). A Jacobian matrix is banded with lower half bandwidth m_l and upper half bandwidth m_u if the ith model equation can be written as

$$\frac{dy_i}{dt} = f_i(y_{i-m_l}, y_{i-m_l+1}, \ldots, y_i, \ldots, y_{i+m_u-1}, y_{i+m_u}), \quad (20)$$

where y_i is the ith dependent variable. The full Jacobian matrix was not banded due to the hydrogen sulfide flux J_i in Eqs. (4) and (19). By neglecting these flux terms only in the Jacobian calculation, the problem became highly banded with $m_l = m_u = 12$. This approximation reduced the number of Jacobian calculations by a factor of 10,000 while having no discernable effect on solution stability or accuracy when tested with smaller cell ensembles. All simulation were performed on a Pentium IV 1.4 GHz processor with 64 MBs of memory.

Specifying meaningful initial conditions for the cell population model was non-trivial due to the very large number of dependent variables. A completely synchronized state in which all cells oscillated with the same period and phase was used as the base case. The synchronization mechanism was evaluated by numerically integrating the population model from various asynchronous initial states generated by

1. Adding random perturbations to the completely synchronized state.
2. Collecting synchronous simulation data over a single oscillation period. The oscillation was divided into M snapshots where the intracellular concentrations were captured. Initial states ranging from completely synchronous to completely asynchronous where each cell was located an equally spaced distance along the oscillatory trajectory were constructed.

While the introduction of random perturbations was simpler to implement, this initialization method did not ensure that a particular cell model has a physiologically meaningful combination of intracellular concentrations. This problem was avoided in the second method by initializing each cell with a set of consistent intracellular concentrations. Random perturbations in intracellular kinetic parameters were used to study synchronization in the presence of small cellular variations.

Numerical integration of the cell population model produced a data matrix which contained the intracellular concentrations of each cell and the extracellular hydrogen sulfide concentration at every sampling point in time. The ensemble average of intracellular variable y at sampling time t_j was calculated as

$$\bar{y}(t_j) = \frac{1}{M}\sum_{i=1}^{M} y_i(t_j). \quad (21)$$

We previously developed a simple method for calculation of the transient cell number distribution for any intracellular variable $z(t)$ (Henson et al., 2002). In this study, we were primarily interested in cell distributions with respect to intracellular hydrogen sulfide and oxygen due to their essential roles in the hypothesized synchronization mechanism. The intracellular species concentration of interest was discretized into L equally spaced bins which covered the full oscillatory range. The number distribution at each sampling time $N(z, t_j)$ was computed by partitioning the cell ensemble into the concentration bins. All distribution calculations were performed using MATLAB. As shown below, achievable resolution was determined by the number of cells (M) in the ensemble and the number of bins L used for discretization. We found that an alternative method based on differentiating the cumulative number distribution (Hukkanen and Braatz, 2003) yielded unacceptable results due to the extreme steepness of the cumulative distribution under highly synchronized conditions.

4. Results and discussion

4.1. Intracellular state initialization studies

The first set of simulation tests were designed to evaluate the hypothesized synchronization mechanism by initializing the cell population to represent various degrees of asynchrony. Each cell ensemble studied was structurally identical in the sense that the same parameter values were employed in every single cell model. Fig. 2 depicts the synchronization of 100 cells where the initial state was constructed by imposing zero mean normally distributed perturbations of variance 1.5 on the nominal intracellular concentrations. The top plot shows the intracellular hydrogen sulfide concentration of each cell and the ensemble average hydrogen sulfide concentration. Corresponding results for intracellular oxygen are shown in the bottom plot. The random perturbations resulted in large initial differences between the single cell oscillation amplitudes and phases. Despite the asynchronous initial state, the cell population became highly synchronized in approximately five oscillations periods.

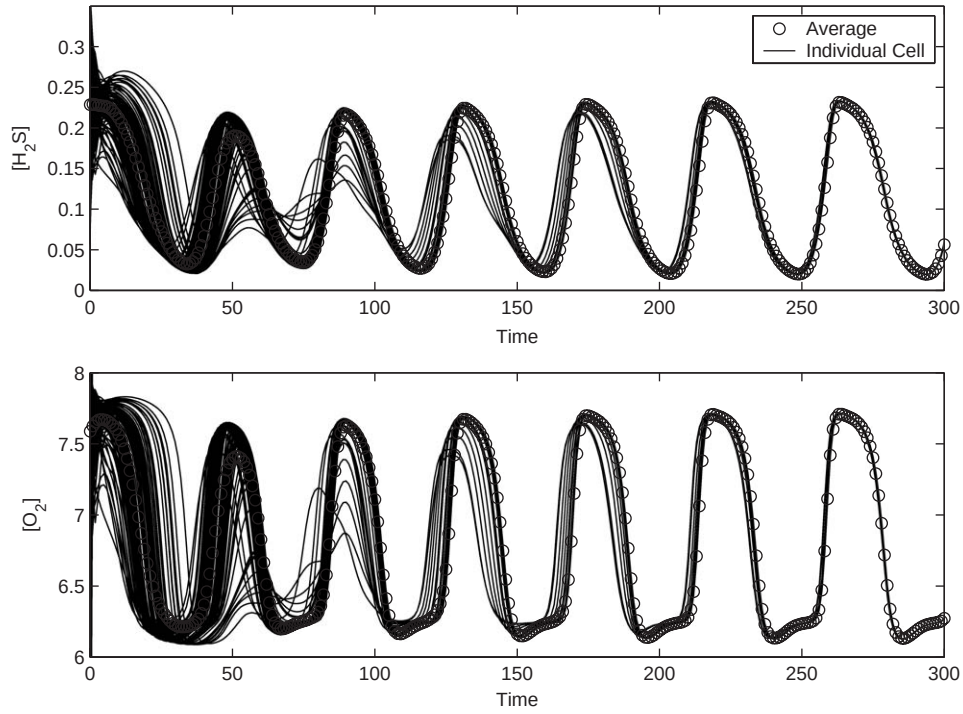

Fig. 2. Synchronization dynamics of a 100 cell ensemble in which the initial state of each cell was perturbed according to a normal distribution with zero mean and a variance of 1.5. The top plot shows the evolution of the hydrogen sulfide concentration of each cell and the ensemble average hydrogen sulfide concentration. The bottom plot shows the evolution of the oxygen concentration of each cell and the ensemble average oxygen concentration.

The effect of 11 important model parameters on the synchronization dynamics of 100 randomly initialized cells is summarized in Table 2. Each parameter was varied ±100% of the nominal value listed in Table 1 while the other parameters were held constant at their nominal values. The simulation results were characterized as follows: (1) the population synchronized slower than with the nominal parameters values (slower synchronization); (2) the population synchronized faster than with the nominal parameters values (faster synchronization); (3) the population exhibited partial synchronization in the sense that a relatively small number of cells failed to synchronize (incomplete synchronization); (4) cells exhibited oscillations but the population did not synchronize (no synchronization); and (5) each cell asymptotically approached the same steady-state solution (steady state). The following conclusions can be drawn from Table 2:

1. An overabundance of extracellular sulfate and/or oxygen inhibits synchronization.
2. A limited range of extracellular ethanol concentrations support synchronization.
3. Synchronization is inhibited by low cell densities.
4. Synchronization requires: (i) a suitable balance of the cysteine production and degradation rates; (ii) a sufficiently small value of the sulfate uptake inhibition constant; and (iii) a sufficiently large value of the respiratory inhibition constant.
5. Synchronization is inhibited by small values of the cellular coupling parameter and large hydrogen sulfide degradation rates.

The effect of the respiratory inhibition parameter is somewhat counterintuitive since larger parameter values produce smaller inhibitory effects. Unfortunately, the experimental data required to validate these model predictions are not currently available.

Fig. 3 shows the effect of cell ensemble size on population dynamics when the initial intracellular concentrations were randomly perturbed as discussed above. To achieve slower synchronization dynamics that better illustrate the effect of ensemble size, the following parameter values were modified from those listed in Table 1: $K_H = 0.25$ and $\kappa = 0.5$. The top plot in Fig. 3 shows the average intracellular hydrogen sulfide concentrations obtained with four different ensemble sizes. The results for two cells demonstrate a potential shortcoming of utilizing very small ensembles to simulate cell population synchronization (Wolf and Heinrich, 1997, 2000). On the other hand, the nearly converged results obtained for 100 and 1000 cells suggest that relatively small ensembles can yield satisfactory predictions of average population behavior.

Table 2
Effect of model parameters on synchronization behavior

Parameter	Description	Value	Result
v_0	Uninhibited sulfate uptake	0.8	Faster synchronization
		1.6	Nominal value
		3.2	Slower synchronization
k_5	Cysteine production constant	0.05	No synchronization
		0.1	Nominal value
		0.2	Faster synchronization
k_6	Cysteine degradation constant	0.06	Steady state
		0.12	Nominal value
		0.24	No synchronization
v_{10}	Oxygen influx	40	Faster synchronization
		80	Nominal value
		160	Slower synchronization
v_{13}	Ethanol uptake	2	No synchronization
		4	Nominal value
		8	Steady state
v_{14}	Oxygen efflux	5	Slower synchronization
		10	Nominal value
		20	Faster synchronization
K_C	Sulfate flux inhibition constant	0.05	Faster synchronization
		0.10	Nominal value
		0.20	No synchronization
K_H	Respiration inhibition constant	0.075	Steady state
		0.15	Nominal value
		0.3	Faster synchronization
ϕ	Cell density	0.05	Incomplete synchronization
		0.1	Nominal value
		0.2	Faster synchronization
κ	Cell coupling parameter	1.0	Slower synchronization
		2.0	Nominal value
		4.0	Faster synchronization
k_{19}	H_2S degradation constant	0.125	Faster synchronization
		0.25	Nominal value
		0.50	Incomplete synchronization

The motivation for utilizing much larger ensembles is high resolution of cell distribution properties. The middle and bottom plots in Fig. 3 show hydrogen sulfide number distributions computed at $t = 140$ and $t = 500$, respectively, for three ensemble sizes. The number of bins used to compute the number distributions were chosen as follows: 100 cells (20 bins), 1000 cells (50 bins) and 10,000 cells (200 bins). While the 100 cell ensemble produced a nearly converged solution for the average intracellular concentration, this relatively small ensemble did not provide satisfactory resolution of the transient cell distribution. For example, the result obtained at $t = 140$ suggests a unimodal distribution. The corresponding results for larger cell ensembles clearly show a bimodal distribution that represents two cell subpopulations which spontaneously emerged from the randomized initial state. Adequate resolution of such cell subpopulations is critical for understanding the emergence and stabilization of yeast autonomous oscillations. For instance, cell cycle related oscillations are characterized by the formation of two subpopulations which represent budded and unbudded cells (Henson, 2003a). Fig. 3 shows that 10,000 cells are required to achieve high resolution of the cell distribution dynamics. The asymmetric distribution obtained at $t = 500$ eventually converged to a very sharp symmetric distribution corresponding to a highly synchronized population.

Corresponding results obtained with completely asynchronous initial states are shown in Fig. 4. The top plot demonstrates that only 10 cells were needed to obtain a converged solution for the average intracellular hydrogen sulfide concentration. Hydrogen sulfide number distributions computed at $t = 0$ and $t = 50$ with the bin numbers chosen as before are shown in the middle and bottom plots, respectively. The 10,000 cell ensemble accurately reproduced the initial bimodal distribution and generated a trimodal distribution at $t = 50$. The bimodal form of the initial distribution is attributable to initialization procedure as equal time spaced sampling produced a large number of cells concentrated near the peak and valley of the synchronous oscillation. A trimodal distribution was temporarily produced during the initial phases of synchronization. The lower and

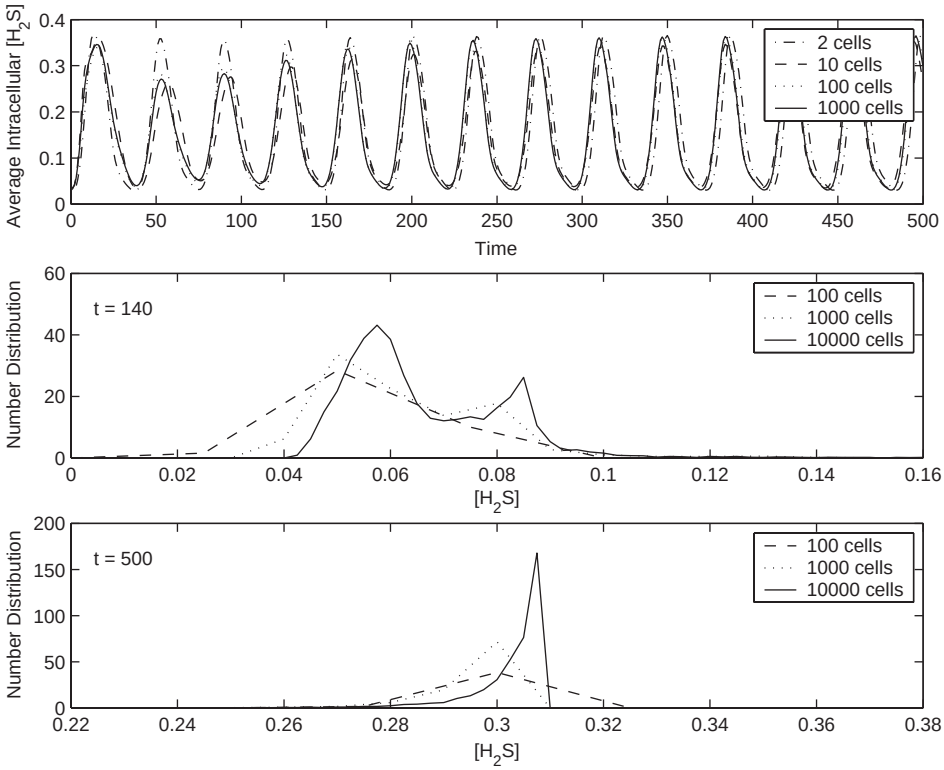

Fig. 3. Synchronization dynamics for five cell ensemble sizes in which the initial state of each cell was perturbed according to a normal distribution with zero mean and a variance of 1.5. The model parameters in Table 1 were used with the exception of $K_H = 0.25$ and $\kappa = 0.5$. The top plot shows average hydrogen sulfide concentrations computed for ensembles containing 2, 10, 100 and 1000 cells. The middle ($t = 140$) and bottom ($t = 500$) plots show hydrogen sulfide number distributions computed for ensembles of 100 cells (20 bins), 1000 cells (50 bins) and 10,000 cells (250 bins).

upper peaks correspond to two cell subpopulations with relatively large amplitude oscillations of different phases. The middle peak represents a third cell subpopulation with relatively small amplitude oscillations that eventually coalesces with the other two subpopulation to produce synchronous oscillations. Such detailed analysis requires the 10,000 cell ensemble as the subpopulations were smeared when smaller ensembles are used as shown in Fig. 4.

The simulation results in Figs. 3 and 4 suggest that 100 cells were sufficient to predict average population dynamics and that 10,000 cells were required for high resolution of distribution properties. Available computational resources limit the number of single cell models that can be included in the ensemble. The following CPU times were obtained for a typical 300 min dynamic simulation on a Pentium IV 1.4 GHz processor with 64 MBs of memory: 100 cells (17 s), 1000 cells (180 s) and 10,000 cells (1680 s). The linear relationship between cell number and computation time was expected because the banded Jacobian option of the ODE solver DVODE was employed. Although results are not presented in this paper, the incorporation of analytical Jacobian calculations had a negligible effect on code efficiency and robustness.

The effect of the initial intracellular state on the synchronization dynamics of a 10,000 cell ensemble is illustrated in Fig. 5. Three initial states ranging from completely asynchronous (100% of the snapshots used for initialization) to relatively synchronized (25% of the snapshots used for initialization) were generated from synchronous simulation data following the procedure described in the previous section. The top plot in Fig. 5 shows the initial hydrogen sulfide number distributions computed with 250 bins. By construction the initial state of the completely asynchronous population (100%) was much disperse than that for the mostly synchronized population (25%). The middle plot which shows ensemble average hydrogen sulfide concentrations clearly demonstrates that the rate of synchronization increased with the degree of initial synchrony. Hydrogen sulfide number distributions computed at $t = 50$ are shown in the bottom plot. As expected, the distribution obtained with the asynchronous initial condition (100%) was considerably more disperse than those obtained with the partially synchronized initial conditions (25% and 50%). The completely asynchronous population (100%) generated a trimodal distribution with three cell subpopulations as discussed above.

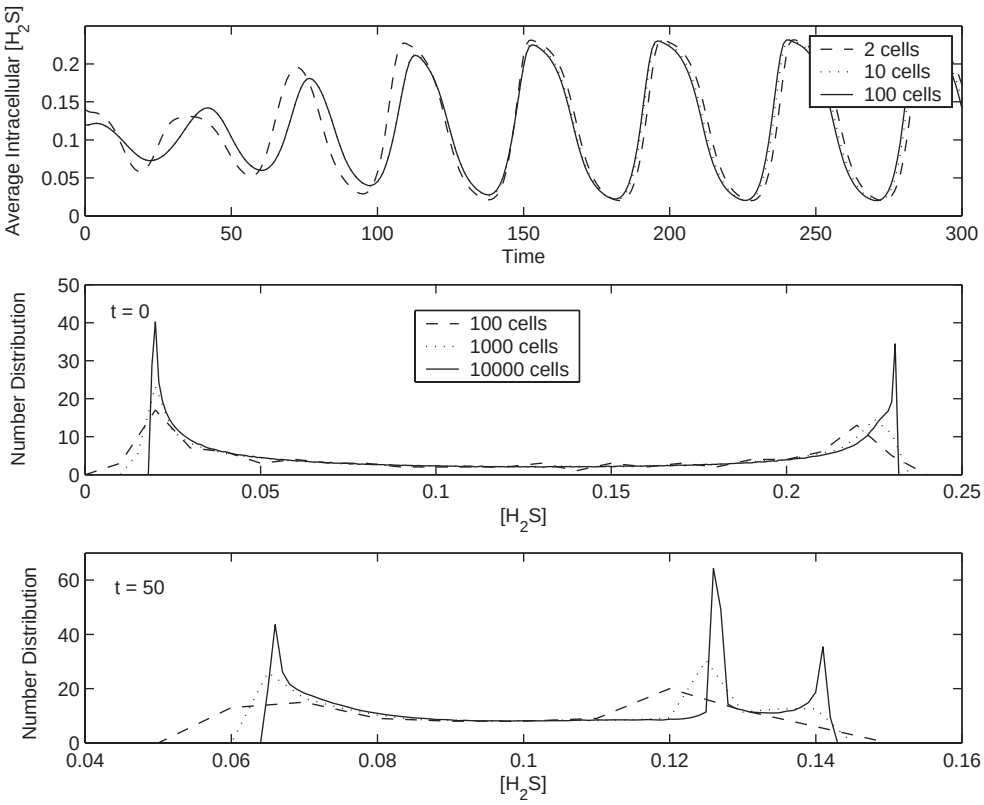

Fig. 4. Synchronization dynamics for five cell ensemble sizes in which completely asynchronous initial states were obtained from synchronous simulation data as explained in the text. The top plot shows average hydrogen sulfide concentrations computed for ensembles containing 2, 10 and 100 cells. The middle ($t = 0$) and bottom ($t = 50$) plots show hydrogen sulfide number distributions computed for ensembles of 100 cells (20 bins), 1000 cells (50 bins) and 10,000 cells (250 bins).

Fig. 6 shows the effect of the respiration inhibition parameter (K_H) on the synchronization dynamics of a 100 cell ensemble. For each K_H value a fully synchronized solution was obtained and used to generate a completely asynchronous intracellular state for initialization of the cell population. Because this parameter determines the inhibitory effect of hydrogen sulfide on oxidative phosphorylation, the simulation results are plotted in terms of the intracellular oxygen concentration. The nominal parameter value ($K_H = 0.15$) produced relatively slow synchronization even though large amplitude single cell oscillations were quickly established. As the K_H value was increased, more rapid synchronization was observed but the time required to achieve fully developed single cell oscillations was substantially longer. Although not shown in Fig. 6, the ensemble average oxygen concentration approached its asymptotic solution most rapidly for the nominal K_H value even though the synchronization dynamics were markedly slower. These results demonstrate a potential limitation of using extracellular and/or average intracellular measurements to investigate the synchronization of cellular oscillations.

The effect of the cell coupling parameter (κ) on the synchronization dynamics of a 100 cell ensemble is illustrated in Fig. 7. For each parameter value investigated a completely asynchronous intracellular state was generated for initialization of the cell population. The top and bottom plots show the evolution of the average intracellular and extracellular hydrogen sulfide concentrations, respectively. Shorter oscillation periods, larger amplitudes in extracellular hydrogen sulfide and more rapid synchronization were observed as the κ value was increased. Because the oscillation period only varied between 44 and 49 dimensionless units over this range of parameter values, κ appears to be a suitable parameter for tuning the cell population model to match data once the necessary synchronization experiments are conducted.

4.2. Intracellular parameter randomization studies

The second set of simulation tests were designed to evaluate the robustness of the proposed synchronization mechanism through the introduction of random perturbations in the single cell model parameters. These tests mimic the effects of cellular variations which result in different expression levels of enzymes controlling the rates of intracellular reactions and membrane transport processes. The nine single cell model parameters

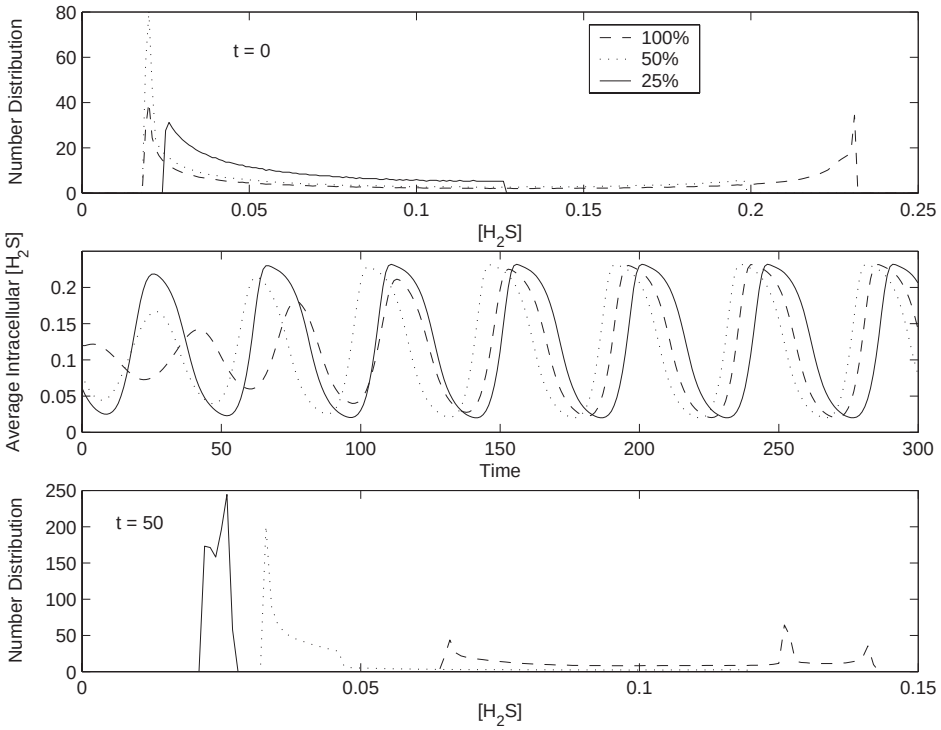

Fig. 5. Synchronization dynamics for three ensembles containing 10,000 cells in which the initial states were obtained from synchronous simulation data as explained in the text. The three initial states correspond to a completely asynchronous population (100% of the synchronous snapshots used), a partially synchronized population (50% of the synchronous snapshots used) and a mostly synchronized population (25% of the synchronous snapshots used). The top plot shows initial hydrogen sulfide number distributions computed with 250 bins. The middle plot shows the evolution of the average intracellular hydrogen sulfide concentrations. The bottom plot shows hydrogen sulfide number distributions computed at $t = 50$.

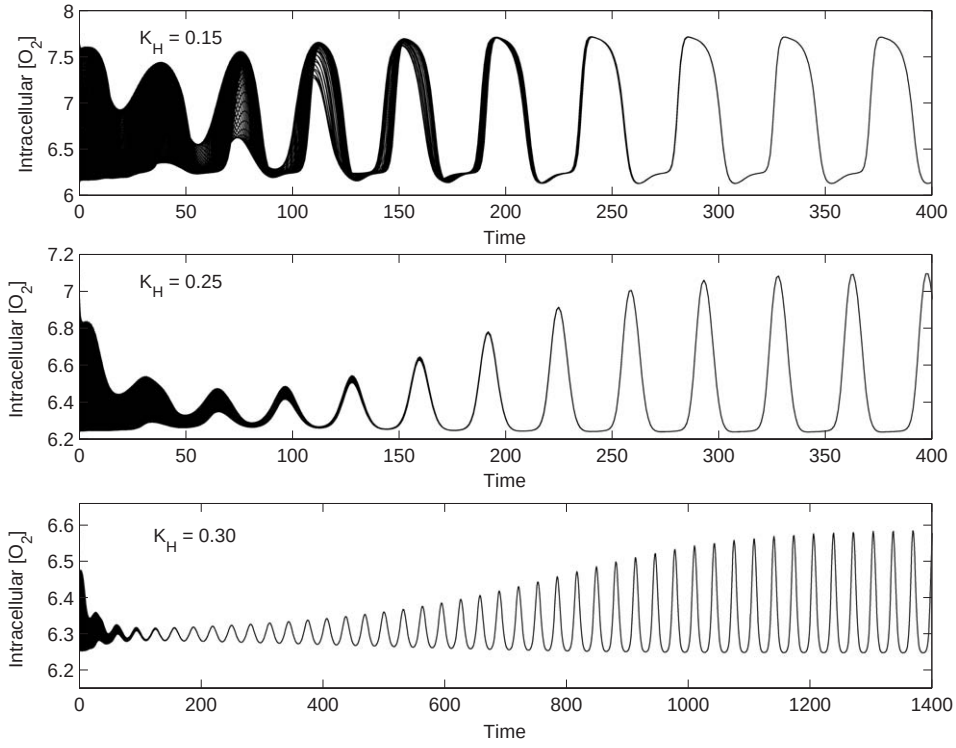

Fig. 6. Effect of the respiration inhibition parameter (K_H) on the synchronization dynamics of ensembles containing 100 cells. A completely asynchronous initial state was generated for each K_H value as described in the text. Each plot shows the evolution of the average intracellular oxygen concentration for a different K_H value.

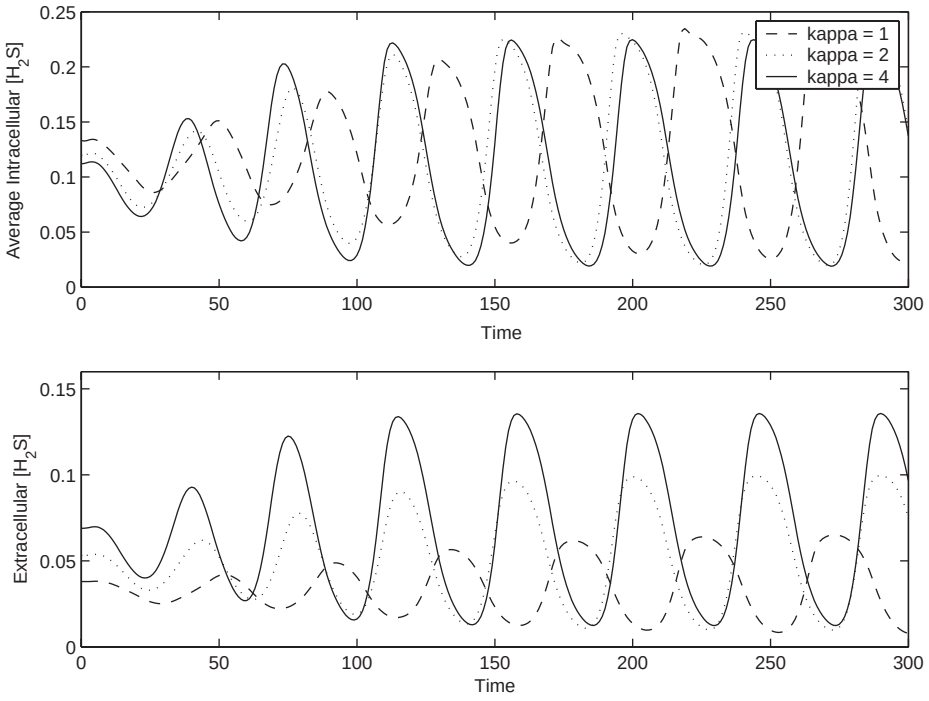

Fig. 7. Effect of the cell coupling parameter (κ) on the synchronization dynamics of ensembles containing 100 cells. A completely asynchronous initial state was generated for each κ value as described in the text. The top and bottom plots show the evolution of the average intracellular and extracellular hydrogen sulfide concentrations, respectively.

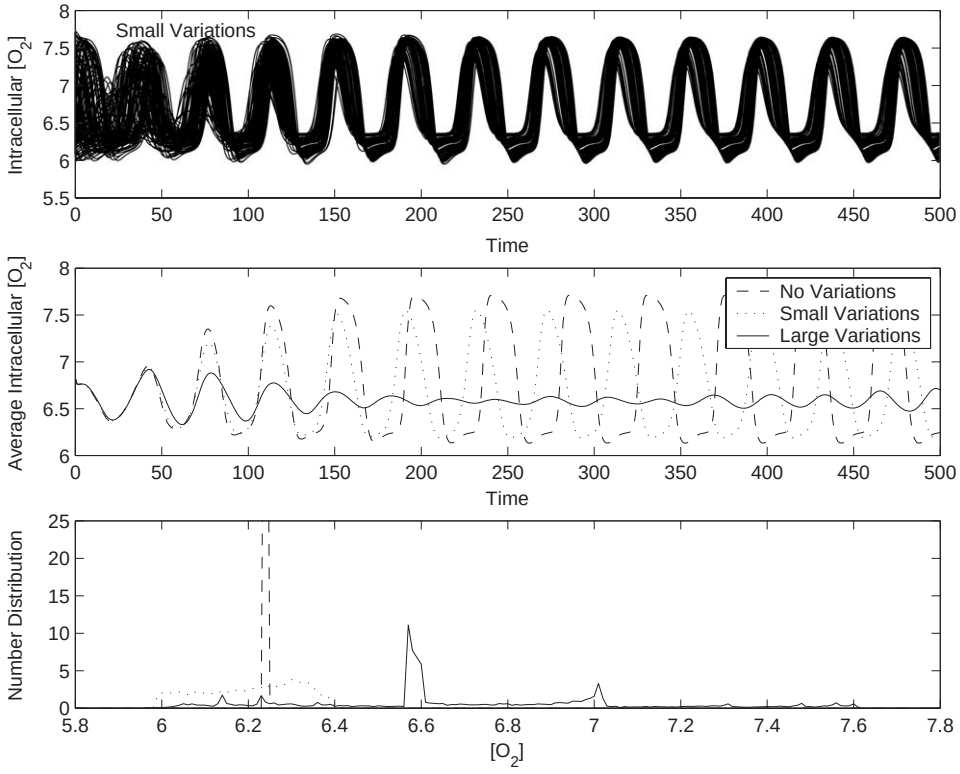

Fig. 8. Effect of random perturbations in selected single cell model parameters on the synchronization dynamics of ensembles containing 10,000 cells. The nine parameters listed in the text were subjected to zero mean normally distributed perturbations with variance 0 (no variations), 0.2 (small variations) and 0.4 (large variations). A completely asynchronous initial state was generated as described in the text. The top plot shows the evolution of 100 representative cells for small parameter variations. The middle plot shows average intracellular oxygen concentrations for the three cases. The bottom plot shows oxygen number distributions computed with 250 bins at $t = 500$.

$(v_0, k_5, k_6, v_{10}, v_{13}, v_{14}, K_C, K_H, \kappa)$ listed in Table 2 were subjected to random perturbations.

The effect of single cell parameter variations on the synchronization dynamics of three ensembles containing 10,000 cells is illustrated in Fig. 8. Zero mean normally distributed perturbations of variance 0 (no variations), 0.2 (small variations) and 0.4 (large variations) were imposed on the nominal parameter values listed in Table 1. The initial condition for each simulation corresponded to a completely asynchronous state. The top plot in Fig. 8 shows the intracellular oxygen concentrations of 100 representative cells when small parameter variations were introduced. A substantial degree of synchronization was achieved despite the cellular variations. The middle plot shows the ensemble average intracellular oxygen concentration for each case. The asymptotic solution for small parameter variations was characterized by a slightly smaller amplitude and a shorter oscillation period than those obtained with no variations. Large parameter variations resulted in very small amplitude oscillations indicative of asynchronous population dynamics. The bottom plot shows oxygen number distributions computed at the final time ($t = 500$) with 250 bins. A distribution consistent with a partially synchronized population was obtained for small parameter variations. By contrast, large variations produced a very dispersed distribution with several distinct cell subpopulations which exhibited different oscillation amplitudes and phases.

Fig. 9 illustrates the effect of the hydrogen sulfide degradation rate on the synchronization dynamics of a 10,000 cell ensemble. This test was designed to simulate experiments in which increased hydrogen sulfide removal from the extracellular environment was achieved by increasing the purge gas flow rate (Keulers et al., 1996a). Experimentally the dissolved oxygen concentration exhibited oscillations of decreasing amplitude as the purge gas flow rate was increased. The authors hypothesized that this behavior was attributable to a lack of population synchronization rather than the absence of single cell oscillations (Keulers et al., 1996a). The simulation test was performed with normally distributed perturbations of variance 0.1 in the single cell model parameters and an initial condition corresponding to a completely asynchronous state. The following step changes in the hydrogen sulfide

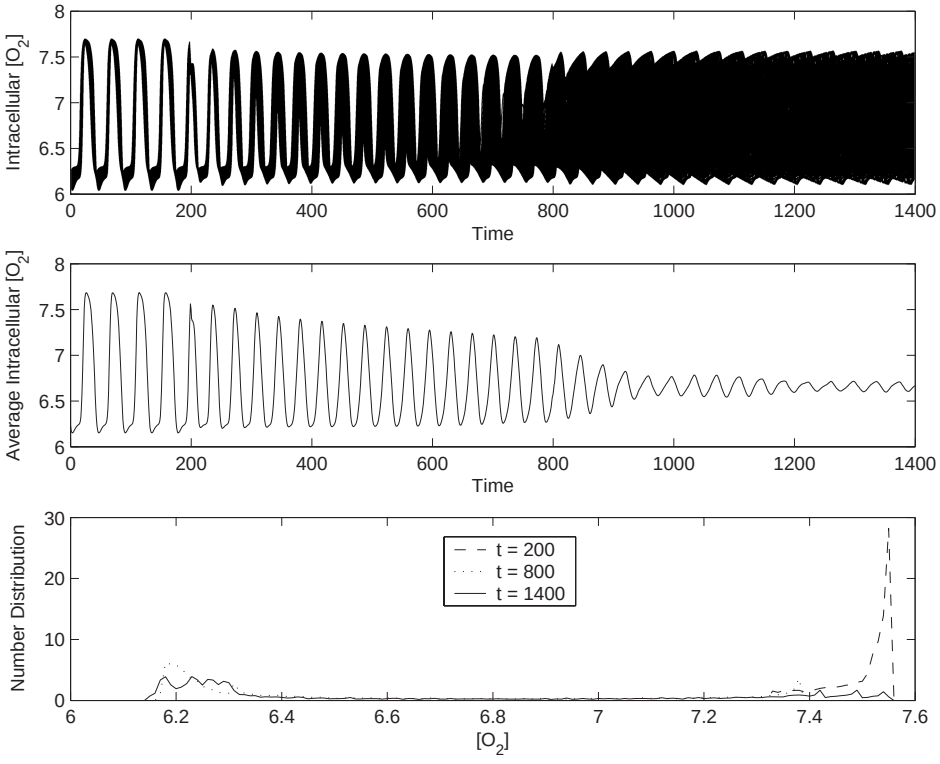

Fig. 9. Effect of the hydrogen sulfide degradation rate on the synchronization dynamics of a 10,000 cell ensemble. The nine single cell model parameters listed in the text were subjected to zero mean normally distributed perturbations with variance 0.1. A completely asynchronous initial state was generated as described in the text. The hydrogen sulfide degradation rate constant was varied as follows: $k_{19} = 0.25$, $0 \leqslant t < 200$; $k_{19} = 1.25$, $200 \leqslant t < 800$; $k_{19} = 6.25$, $800 \leqslant t \leqslant 1400$. The top and middle plots show the intracellular oxygen concentrations of 100 representative cells and the average intracellular oxygen concentration, respectively. The bottom plot shows oxygen number distributions computed with 200 bins at $t = 200$, 800 and 1400.

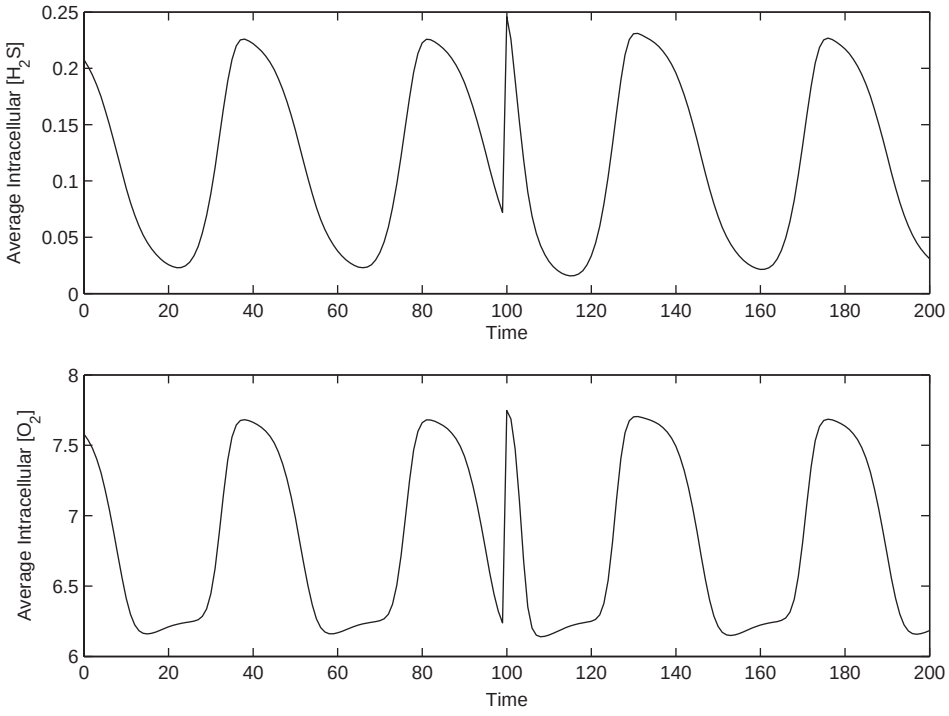

Fig. 10. Effect of an extracellular hydrogen sulfide pulse on the synchronization dynamics of a 100 cell ensemble. The nine single cell model parameters listed in the text were subjected to zero mean normally distributed perturbations with variance 0.1. An initial condition corresponding to a completely synchronous state was used. The extracellular hydrogen sulfide concentration was instantaneously increased by 800%. The top and middle plots show the average intracellular hydrogen sulfide and oxygen concentrations, respectively.

degradation rate constant were implemented: $k_{19} = 0.25$, $0 \leqslant t < 200$; $k_{19} = 1.25$, $200 \leqslant t < 800$; $k_{19} = 6.25$, $800 \leqslant t \leqslant 1400$.

The top plot in Fig. 9 shows the intracellular oxygen concentrations of 100 representative cells. While substantial population desynchronization was observed with increasing k_{19} value, the amplitude of single cell oscillations were not strongly affected. The evolution of the average intracellular oxygen concentration shown in the middle plot is qualitatively similar to the dissolved oxygen concentration response measured in the purge gas flow rate experiments (Keulers et al., 1996a). The bottom plot shows intracellular oxygen number distributions computed with 200 bins immediately before the two k_{19} changes ($t = 200, 800$) and at the final time ($t = 1400$). Progressive desynchronization of the cell population is clearly evident from the computed distributions. This simulation result supports the hypothesis that large purge gas flow rates cause the loss of macroscopically observable oscillations through population desynchronization rather than by elimination of oscillations at the single cell level.

The effect of a hydrogen sulfide pulse on the synchronization dynamics of a 100 cell ensemble is illustrated in Fig. 10. The simulation was performed with randomly distributed perturbations of variance 0.1 in the single cell model parameters and an initial condition corresponding to a completely synchronous state. At $t = 100$ the extracellular hydrogen sulfide concentration was instantaneously increased by 800% and then allowed to decay to its normal level through the effect of extracellular degradation. This test was designed to mimic experiments in which the extracellular hydrogen sulfide concentration was suddenly increased by injection of sodium sulfide (Sohn et al., 2000). The top and bottom plots in Fig. 10 show ensemble average values of the intracellular hydrogen sulfide and oxygen concentrations, respectively. As observed experimentally (Sohn et al., 2000), the sustained oscillations were only briefly perturbed before quickly returning to their unperturbed forms. The similarity between the experimental and simulated responses provides further support for the proposed synchronization mechanism.

5. Summary and conclusions

A cell population model was developed to investigate a hydrogen sulfide mediated mechanism proposed for the synchronization of yeast respiratory oscillations. A recently published single cell model was modified to include hydrogen sulfide transport across the cell membrane and degradation in the extracellular environment. The cell population model was formulated by

coupling a large ensemble of single cell models to a mass balance for extracellular hydrogen sulfide. A variety of dynamic simulation tests were performed to investigate the effect of the initial intracellular state and intracellular kinetic parameter variations on synchronization dynamics. The cell population model was shown to generate synchronous oscillations for a wide range of model parameter values. Approximately 100 cells were required to obtain converged solutions for average intracellular concentrations, while ensembles containing 10,000 cells were shown to be advantageous for computing transient number distributions. The cell population model was shown to provide qualitative agreement with synchronization experiments presented in literature.

The simulation results provide important insights into the synchronization of cellular oscillators that are chemically coupled by intracellular species such as hydrogen sulfide which are transported across the cell membrane. An appropriate balance between the membrane transport rate and the rate at which the coupling species is removed from the extracellular environment is required to maintain the coupling species extracellular concentration within the range that supports synchronization. Another general conclusion pertains to feedback inhibiting metabolites such as cysteine which are responsible for single cell oscillations. Synchronization requires a suitable balance between the production and degradation rates of the feedback inhibiting metabolite such that its intracellular concentration is maintained within a certain range.

The proposed modeling framework is broadly applicable to synchronization problems in other cellular systems which are not amenable to analytical treatment (Mirollo and Strogatz, 1990). We have previously used the cell ensemble approach to investigate yeast glycolytic oscillations mediated by the coupling species acetaldehyde (Henson et al., 2002). Although considerably more complex due to the interaction between cell cycle progression and energy and storage carbohydrate metabolism, yeast cell cycle oscillations can also be investigated with the proposed methodology by viewing ethanol as the coupling species (Nielsen and Villadsen, 1994). Another potential application is the synchronization of circadian oscillators governed by gene regulatory networks (Leloup and Goldbeter, 1998). Such studies are the subject of our future research.

References

Aon, M.A., Cortassa, S., Westerhoff, H.V., van Dam, K., 1992. Synchrony and mutual stimulation of yeast cells during fast glycolytic oscillations. J. Gen. Microbiol. 138, 2219–2227.

Bier, M., Bakker, B.M., Westerhoff, H.V., 2000. How yeast cells synchronize their glycolytic oscillations: a perturbation analytic treatment. Biophys. J. 78, 1087–1093.

Brown, P.N., Byrne, G.D., Hindmarsh, A.C., 1989. VODE: a variable coefficient ODE solver. SIAM J. Sci. Stat. Comput. 10, 1038–1051.

Das, J., Busse, H.-G., 1991. Analysis of the dynamics of relaxation type oscillation in glycolysis of yeast extracts. Biophys. J. 60, 363–379.

Domach, M.M., Shuler, M.L., 1984. A finite representation model for an asynchronous culture of *E. coli*. Biotech. Bioeng. 26, 877–884.

Fredrickson, A.G., Ramkrishna, D., Tsuchiya, H.M., 1967. Statistics and dynamics of procaryotic cell populations. Math. Biosci. 1, 327–374.

Ghosh, A., Chance, B., 1964. Oscillations for glycolytic intermediates in yeast cells. Biochem. Biophys. Res. Commun. 16, 174–181.

Ghosh, A.K., Chance, B., Pye, E.K., 1971. Metabolic coupling and synchronization of NADH oscillations in yeast cell populations. Arch. Biochem. Biophys. 145, 319–331.

Henson, M.A., 2003a. Dynamic modeling and control of yeast cell populations in continuous biochemical reactors. Comput. Chem. Eng. 27, 1185–1199.

Henson, M.A., 2003b. Dynamic modeling of microbial cell populations. Curr. Opin. Biotechnol. 14, 460–467.

Henson, M.A., 2004. Cell population modeling of autonomously oscillating yeast cultures. Comput. Chem. Eng., in press.

Henson, M.A., Muller, D., Reuss, M., 2002. Cell population modeling of yeast glycolytic oscillations. Biochem. J. 368, 433–446.

Hjortso, M.A., Nielsen, J., 1995. Population balance models of autonomous microbial oscillations. J. Biotech. 42, 255–269.

Hukkanen, E.J., Braatz, R.D., 2003. Measurement of particle size distribution in suspension polymerization using *in situ* laser backscattering. Sensors Actuators B 96, 451–459.

Keulers, M., Kuriyama, H., 1998. Extracellular signaling in an oscillatory yeast culture. In: Holcombe, W.M.L., Paton, R., Holcombe, M. (Eds.), Information Processing in Cells and Tissues. Plenum, New York, pp. 85–94.

Keulers, M., Satroutdinov, A.D., Suzuki, T., Kuriyama, H., 1996a. Synchronization affector of autonomous short-period-sustained oscillation of *Saccharomyces cerevisiae*. Yeast 12, 673–682.

Keulers, M., Suzuki, T., Satroutdinov, A.D., Kuriyama, H., 1996b. Autonomous metabolic oscillations in continuous culture of *Saccharomyces cerevisiae* grown on ethanol. FEMS Microbiol. Lett. 142, 253–258.

Kim, B.G., Shuler, M.L., 1990. A structured, segregated model for genetically modified *Escherichia coli* cells and its use for prediction of plasmid stability. Biotech. Bioeng. 36, 581–592.

Leloup, J.-C., Goldbeter, A., 1998. A model for circadian rhythms in *Drosophila* incorporating the formation of a complex between the PER and TIM proteins. J. Biol. Rhythms 13, 70–87.

Mirollo, R.E., Strogatz, S.H., 1990. Synchronization of pulse-coupled biological oscillators. SIAM J. Appl. Math. 50, 1645–1662.

Muller, D., Exler, S., Aguilera-Vazquez, L., Guerrero-Martin, E., Reuss, M., 2003. cAMP mediates the cell cycle dynamics of *Saccharomyces cerevisiae*. Yeast 20, 351–367.

Murray, D.B., Roller, S., Kuriyama, H., Lloyd, D., 2001. Clock control of ultradian respiratory oscillations found during yeast continuous culture. J. Bacteriol. 183, 7253–7259.

Nielsen, J., Villadsen, J., 1994. Bioreaction Engineering Principles. Plenum Press, New York.

Parulekar, S.J., Semones, G.B., Rolf, M.J., Lievense, J.C., Lim, H.C., 1986. Induction and elimination of oscillations in continuous cultures of *Saccharomyces cerevisiae*. Biotech. Bioeng. 28, 700–710.

Richard, P., Diderich, J.A., Bakker, B.M., Teusink, B., van Dam, K., Westerhoff, H.V., 1994. Yeast cells with a specific cellular make-up and an environment that removes acetaldehyde are prone to sustained glycolytic oscillations. FEBS Lett. 341, 223–226.

Richard, P., Bakker, B.M., Teusink, B., van Dam, K., Westerhoff, H.V., 1996. Acetaldehyde mediates the synchronization of

sustained glycolytic oscillations in populations of yeast cells. Eur. J. Biochem. 235, 238–241.

Satroutdinov, A.D., Kuriyama, H., Kobayashi, H., 1992. Oscillatory metabolism of *Saccharomyces cerevisiae* in continuous culture. FEMS Microbiol. Lett. 98, 261–268.

Sohn, H.-Y., Kuriyama, H., 2001. Ultradian metabolic oscillation of *Saccharomyces cerevisiae* during aerobic continuous culture: hydrogen sulfide, a population synchronizer, is produced by sulphite reductase. Yeast 18, 125–135.

Sohn, H.-Y., Murray, D.B., Kuriyama, H., 2000. Ultradian oscillation of *Saccharomyces cerevisiae* during aerobic continuous culture: hydrogen sulfide mediates population synchrony. Yeast 16, 1185–1190.

von Meyenburg, H.K., 1973. Stable synchrony oscillations in continuous culture of *Saccharomyces cerevisiae* under glucose limitation. In: Chance, B., Pye, E.K., Shosh, A.K., Hess, B. (Eds.), Biological and Biochemical Oscillators. Academic Press, New York, pp. 411–417.

Wolf, J., Heinrich, R., 1997. Dynamics of two-component biochemical systems in interacting cells: synchronization and desynchronization of oscillations and multiple steady states. Biosystems 43, 1–24.

Wolf, J., Heinrich, R., 2000. Effect of cellular interaction on glycolytic oscillations in yeast: a theoretical investigation. Biochem. J. 345, 321–334.

Wolf, J., Passarge, J., Somsen, O.J.G., Snoep, J.L., Heinrich, R., Westerhoff, H.V., 2000. Transduction of intracellular and intercellular dynamics in yeast glycolytic oscillations. Biophys. J. 78, 1145–1153.

Wolf, J., Sohn, H.-Y., Heinrich, R., Kuriyama, H., 2001. Mathematical analysis of a mechanism for autonomous metabolic oscillations in continuous culture of *Saccharomyces cerevisiae*. FEBS Lett. 499, 230–234.